

Bi₄Br₄-based saturable absorber with robustness at high power for ultrafast photonic device

Cite as: Appl. Phys. Lett. **120**, 053108 (2022); <https://doi.org/10.1063/5.0077148>

Submitted: 31 October 2021 • Accepted: 25 January 2022 • Published Online: 03 February 2022

 Wenjun Liu, Xiaolu Xiong, Mengli Liu, et al.

COLLECTIONS

Paper published as part of the special topic on [One-Dimensional van der Waals Materials](#)



View Online



Export Citation



CrossMark

ARTICLES YOU MAY BE INTERESTED IN

[Controllable epitaxy of quasi-one-dimensional topological insulator \$\alpha\$ -Bi₄Br₄ for the application of saturable absorber](#)

Applied Physics Letters **120**, 093103 (2022); <https://doi.org/10.1063/5.0083807>

[Efficient modulation of MoS₂/WSe₂ interlayer excitons via uniaxial strain](#)

Applied Physics Letters **120**, 053107 (2022); <https://doi.org/10.1063/5.0078073>

[Thickness dependence of quantum transport in the topological superconductor candidate SnTaS₂](#)

Applied Physics Letters **120**, 053102 (2022); <https://doi.org/10.1063/5.0080851>

Lock-in Amplifiers
up to 600 MHz



Zurich
Instruments



Bi₄Br₄-based saturable absorber with robustness at high power for ultrafast photonic device

Cite as: Appl. Phys. Lett. **120**, 053108 (2022); doi: [10.1063/5.0077148](https://doi.org/10.1063/5.0077148)

Submitted: 31 October 2021 · Accepted: 25 January 2022 ·

Published Online: 3 February 2022



View Online



Export Citation



CrossMark

Wenjun Liu,^{1,2}  Xiaolu Xiong,^{3,4} Mengli Liu,¹ XiaoWei Xing,¹  Hailong Chen,² Han Ye,¹ Junfeng Han,^{3,4,a)}  and Zhiyi Wei^{2,a)}

AFFILIATIONS

¹State Key Laboratory of Information Photonics and Optical Communications, School of Science, P. O. Box 91, Beijing University of Posts and Telecommunications, Beijing 100876, China

²Beijing National Laboratory for Condensed Matter Physics, Institute of Physics, Chinese Academy of Sciences, Beijing 100190, China

³Centre for Quantum Physics, Key Laboratory of Advanced Optoelectronic Quantum Architecture and Measurement (MOE), School of Physics, Beijing Institute of Technology, Beijing 100081, China

⁴Yangtze Delta Region Academy of Beijing Institute of Technology, Jiaxing 314000, China

Note: This paper is part of the APL Special Collection on One-Dimensional van der Waals Materials.

a) Authors to whom correspondence should be addressed: pkuhjf@bit.edu.cn and zywei@iphy.ac.cn

ABSTRACT

Saturable absorption may be induced at critical pumping power by nonlinear optical effects of nanomaterials, thereby making it possible to generate a high-power ultrafast laser. Recently, Bi₄Br₄ is theoretically predicted to be a member of topological insulators and is expected to be a promising candidate for saturable absorbers (SAs). We show here that Bi₄Br₄ features a large modulation depth of 42.3%. The Bi₄Br₄-based SA enables mode-locking operation at the near-infrared range, as demonstrated here by a 1.5 μm fiber laser with a signal-to-noise ratio (SNR) of 90 dB and a pulse duration of 172 fs. Moreover, the robustness of the Bi₄Br₄-based SA at relatively high power is of particular interest, which can be proved by a laser's stable operation state. The strong optical nonlinearity and robustness provided by Bi₄Br₄ may arouse a growing upsurge in the innovation of high-power ultrafast photonic devices and further development of photon applications.

Published under an exclusive license by AIP Publishing. <https://doi.org/10.1063/5.0077148>

Ultrafast lasers afford high pulse instantaneous intensity, repetition rate, and temporal and spatial resolution, which are essential in the research of laser microsurgery, bioimaging, large-capacity optical communication, and high-precision material processing.^{1–6} After years of development, mature passively mode-locking technology has been considered to be one of the most effective technologies in the formation of ultrafast pulses.^{7–11} The core of this technology is the nonlinear optical (NLO) modulation device, which exhibits absorption saturation owing to its nonlinear interaction with light and is often called the saturable absorber (SA).¹² So far, this kind of absorption saturation involving fast relaxation of valence or conductive electrons has been observed in various materials.^{13–16} Generally speaking, an ideal saturable absorber is expected to have narrow bandgap for broadband applications and strong nonlinearity and fast relaxation time for effective pulse narrowing. Therefore, the nanomaterials with a low dimensional structure have become the main choice due to their excellent photoelectric properties.^{17–20} For instance, gapless materials graphene exhibits ultrafast carrier relaxation process, high damage threshold, and

broadband absorption in the application of lasers. At the same time, the narrow bandgap means that the material can realize the application of a higher band mode-locked fiber laser.²¹ The narrow bandgap materials have some excellent research results around the 2 μm band.²² Most of the valued properties are attributed to its Dirac cone structure. On the one hand, as the density of states is small, it is easy to achieve saturation absorption. On the other hand, the carrier relaxation speed is fast in this structure, which is conducive to the construction of the ultrafast fiber laser. However, the absorption of single-layer graphene is limited, which will affect the efficiency of the laser output.²³ Although the multilayer graphene can enhance the absorption of light, it can inevitably bring loss, which affects the performance such as the output power of the laser.²⁴

In recent years, a kind of graphene-like Dirac material called topological insulators (TIs) with narrow bandgap and metallic surfaces or edge states has aroused a worldwide research upsurge.²⁵ As the bandgap of TIs is small, the applicable spectral range can be extended to mid-infrared. Meanwhile, the surface state with Dirac cones can

rapidly enhance its relaxation speed.²⁶ Therefore, it has great potential in saturable absorption. Due to the excellent strong optical nonlinearity and broadband saturable absorption, TIs have been regarded as another promising and powerful candidate for ultrafast pulse generation.²⁷ Recently, Bi_4Br_4 is theoretically predicted to be a member of topological insulators and is expected to be a promising candidate for multichannel dissipationless electronic devices.^{28,29} The bandgap of monolayer Bi_4Br_4 is reported to be $\sim 0.2\text{ eV}$ with gapless edge

states,^{30,31} which indicates that it has the potential to exhibit absorption properties in the near infrared and even wider range.

In this contribution, nonlinear optical properties of Bi_4Br_4 have been specifically investigated through experiments. The Bi_4Br_4 SA is prepared via a self-flux method,³² which is an effective method to grow crystal materials. Before being applied to the laser, the Bi_4Br_4 SA is found to exhibit an attractive nonlinear absorption, the saturation intensity, and the modulation depth of which are 0.55 MW/cm^2 and

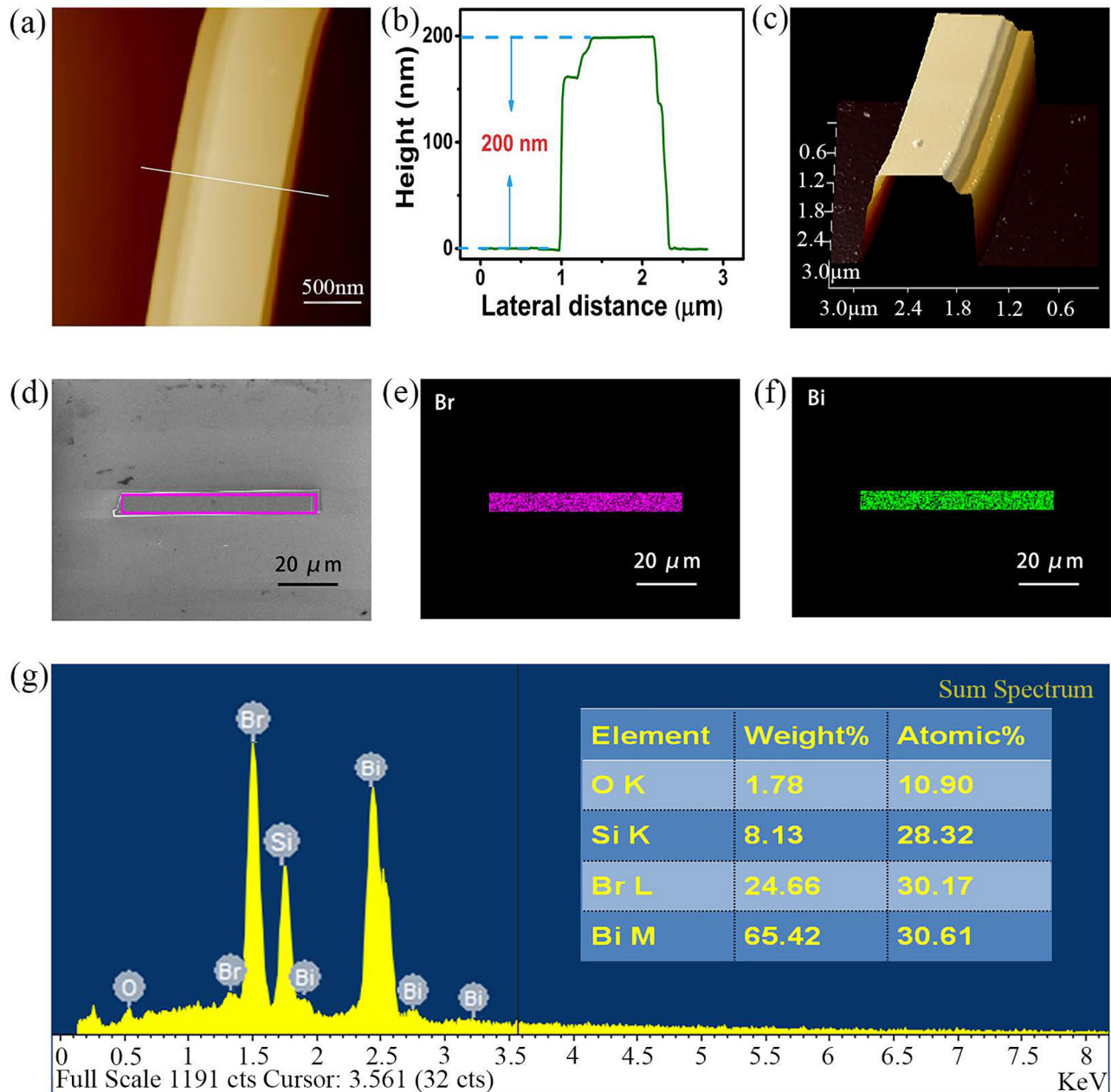


FIG. 1. The AFM, SEM, and EDS of the Bi_4Br_4 nanobelt. (a) Topography of exfoliated Bi_4Br_4 recorded in the scanasyst mode. (b) AFM height profile taken along the green line in (a). (c) 3D image of exfoliated Bi_4Br_4 . (d) SEM of exfoliated Bi_4Br_4 . (e) The element mapping of Br. (f) The element mapping of Bi. (g) EDS spectrum of Bi_4Br_4 .

42.3%, respectively. Furthermore, the laser integrated with the Bi_4Br_4 SA has been demonstrated to produce ultrafast pulses with a pulse duration of 172 fs. The SNR up to 90 dB and the output power of 20 mW illustrate the stability of the Bi_4Br_4 SA in continuous operation at high power. The excellent performance of Bi_4Br_4 as a SA in the laser illustrates its potential value in expanding effective nonlinear photonic devices, which may bring down to the further practical application of Bi_4Br_4 and the innovation of ultrafast photons.

Figures 1(a)–1(c) illustrate the morphology and three-dimensional image of Bi_4Br_4 , respectively. The typical line profile is shown in Fig. 1(b), which shows that the material has a thickness of about 200 nm. Most of the area on the top surface are flat along with several steps at the edge. The topography of Bi_4Br_4 was recorded by a scanning electron microscope (SEM), as shown in Fig. 1(d). The element mapping of Br and Bi is shown in Figs. 1(e) and 1(f). The energy dispersive x-ray spectrum in Fig. 1(g) reveals that the peak of atoms Bi, Br, Si, O, and Si, O originates from substrates. The actual composition of the sample listed in Fig. 1 indicates that the Bi/Br atomic ratio is 1:1.

In Fig. 2, the Bi_4Br_4 flakes and SA are characterized. The bright-field transmission electron microscopy (TEM) image of the Bi_4Br_4 flake is shown in Fig. 2(a). The flake is continuous and homogeneous in a large scale. Figure 2(b) shows a high-resolution image of the Bi_4Br_4 crystal lattice. The measured lattice distance from the TEM image is 4.2 Å, corresponding to the direction of Bi_4Br_4 single crystals

in Fig. 2(c). Then, the x-ray diffraction (XRD) peaks were collected as shown in Fig. 2(d). The main diffraction peaks can be indexed as the (00l) reflections of $\alpha\text{-Bi}_4\text{Br}_4$, suggesting that the measured plane is in the ab plane.

The power-dependent nonlinear transmission of the Bi_4Br_4 -based SA is measured by a mode-locked fiber laser (MLFL) featuring a repetition rate of 120 MHz and a pulse duration of 700 fs at 1.5 μm . The measured data in Fig. 2(e) are fitted by a widely accepted standard two-level saturable absorber model. With 800 nm excitation light and 5 μm probe light, we get the experimental data as shown as the orange dot in Fig. 2(f). After performing a fitting analysis with multiple-exponential functions, the relaxation is decomposed into two decay components: an ultrafast component with a characteristic time of 200 fs and a fast component with a characteristic time of 3.2 ps. As the photon energy of the pump and probe light are larger than the bandgap of Bi_4Br_4 (0.2 eV), both of them can cause inter-band transfer of electrons.

The balanced twin-detector method can be shown in Fig. 3(a). The modulation depth, saturation intensity, and non-saturable absorption loss of the Bi_4Br_4 SA are measured by this method.³² The pulse source is a homemade 125 MHz fiber laser centered at 1550 nm with 100 fs pulse duration and 80 mW output power. A variable optical attenuator (VOA) is used to control the power level of the optical pulses. A 50:50 optical coupler (OC) is applied to divide the incident optical pulses into two paths with the same power. The main function

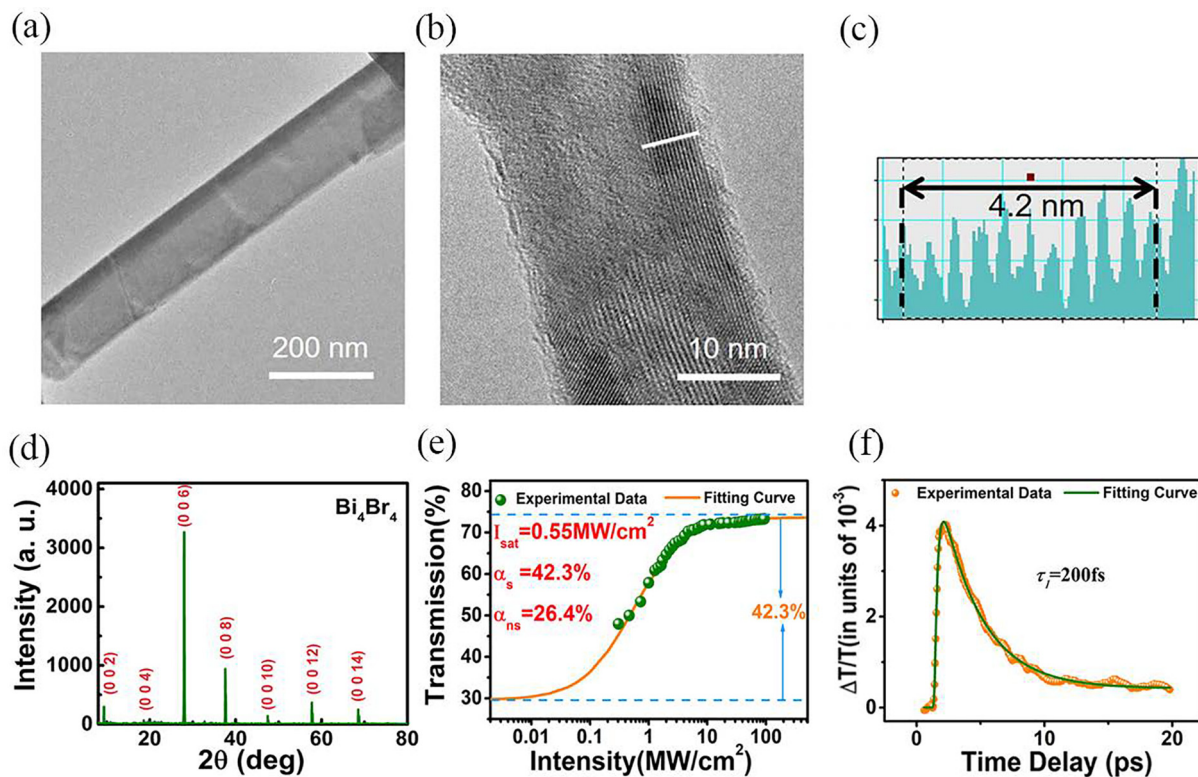


FIG. 2. The TEM, XRD, and nonlinear transmission of the Bi_4Br_4 flakes from the same single crystal. (a) Bright field TEM image of the $\alpha\text{-Bi}_4\text{Br}_4$ nanobelt. (b) High resolution TEM image obtained from the top of the $\alpha\text{-Bi}_4\text{Br}_4$ nanobelt. (c) The distance of the lattice is about 4.2 Å. (d) XRD of Bi_4Br_4 flakes with the c axis coaligned normal to the sample holder under ambient conditions. (e) The power-dependent nonlinear transmission of the Bi_4Br_4 -based SA. (f) Measured transmittivity transients of Bi_4Br_4 .

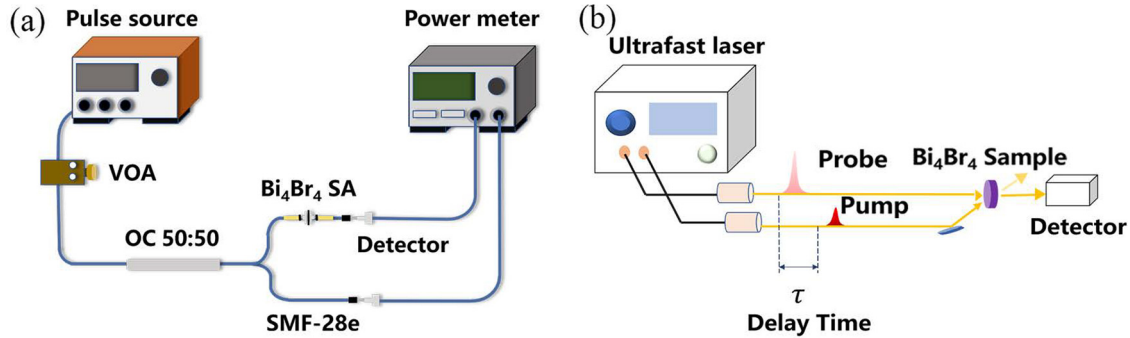


FIG. 3. The setup for measuring nonlinearity. (a) Schematic diagram of the saturable absorption measurement. VOAs: variable optical attenuators; OC: optical coupler. (b) The pump-probe measurements.

of the circulator is to pass optical pulses through the SA mirror with a spatial structure. By rotating the VOA, we can measure the different output power from high to low at two detectors. Based on the measured data, we can fit the saturable absorption of the Bi_4Br_4 SA, as described by the model

$$\alpha(I) = \frac{\alpha_s}{1 + I/I_{\text{sat}}} + \alpha_{\text{ns}},$$

where α_s is the modulation depth (saturable loss), α_{ns} is the nonsaturable loss, and I_{sat} is the saturable intensity. The performance difference of the transmission rate under different power presents a modulation depth (α_s) of 42.3%; meanwhile, the saturable intensity (I_{sat}) and nonsaturable loss (α_{ns}) are assessed as 0.55 MW/cm^2 and 26.4%, respectively. The modulation depth of the Bi_4Br_4 -based SA higher than other saturable materials reveals the strong nonlinearity of Bi_4Br_4 and its potential as a modulation device. A small insertion loss of 1.3 dB is also acceptable for its further laser applications. The time-resolved pump-probe profiles of Bi_4Br_4 are obtained using a femtosecond laser system.³³ Such a setup of the pump-probe analyses can help us to understand the decay process related to inter-band recombination in Bi_4Br_4 in Fig. 3(b). There, we can assume that the response time is sufficient as an ultrafast saturated absorber.

Inspired by the research of the MLFL near $2 \mu\text{m}$, we predict that Bi_4Br_4 has the potential to exhibit absorption characteristics in the near infrared or even wider range.³⁴ By the notable saturable absorption properties previously shown, it is quite promising to establish the mode-locked laser using the Bi_4Br_4 -based SA. The experimental schematic diagram of a ring cavity laser employing the Bi_4Br_4 -based SA is displayed in Fig. 4(a). A laser diode (LD) operating at 980 nm is to pump the 0.5 m long gain medium commercial erbium doped fiber (EDF) via a 980/1550 nm wavelength-division multiplexer (WDM). The function of the polarization controller (PC) is to alter the polarization state of light to optimize the working state. To implement the operation of unidirectional traveling, an isolator (ISO) is integrated into the laser cavity. 20% of the laser light are extracted from the cavity via a fiber optical coupler (OC) for real-time observation and measurement. In order to avoid the measurement error caused by different samples, only one flake is used during the experiment in the fiber laser. The flakes, which are exfoliated from the same single crystal with the same thickness, are used in the measurement of the saturable absorption and pump-probe. The pulse sequence is monitored in real time

by an oscilloscope (Tektronix DPO 3054), the autocorrelator (APE Pulse check), an optical spectrum analyzer (Yokogawa AQ 6370C), and a RF spectrum analyzer (Rohde& Schwarz FSW26) are used for further measurement of the acquired mode-locked signals.

By properly adjusting the pump power and fine-tuning the PC, a mode-locking phenomenon is observed on the oscilloscope at the pump power of 234 mW. The time interval between two pulses in Fig. 4(b) is 20 ns, which is in good agreement with the repetition frequency of 49.92 MHz. Figure 4(c) illustrates the optical spectrum of mode-locking centered at 1559.23 nm and shows a 3-dB bandwidth about 23.26 nm. With the naked eye, the spectra sampled every four hours maintain good consistency in shape. Figure 4(d) presents the first peak of the radio frequency (RF) spectrum appearing at 49.92 MHz. By comparing the maximum value of the peak and the background value, the SNR is calculated to be 90 dB. The RF sequences in the illustration are uniformly arranged without spectral modulation over a wide range, indicating the well operation of lasers. Long-term spectrum monitoring and high SNR make us confident of the stability of this mode-locked system. The autocorrelation trace is recorded in Fig. 4(e). The soliton generated in the laser is generally approximated as a hyperbolic secant. As a result, the curve fitting the experimental data with the Sech^2 intensity profile reveals a pulse duration of 172 fs.

To investigate the performance of the Bi_4Br_4 -based SA at high power, the pump power is controlled within a suitable range. In the process of gradually increasing the pump power from 234 mW to 630 mW, the intensity of the mode-locked sequences measured by the power meter is significantly increased as shown in Fig. 4, which indicates that the mode-locking laser shows superior robustness. Due to the higher pump power (630 mW) and lower nonsaturable loss (26.4%), the final output power of the MLFL is recorded as 20 mW.

Moreover, the relationship curve between the pump power and output power shows almost constant slope, and no signal of fading is observed in the later stages of high power as shown in Fig. 4(f). Hence, one can see that the Bi_4Br_4 -based SA is expected to maintain stable nonlinear absorption at higher powers. Furthermore, the long-term jitter of the laser at the highest pump power is monitored at a frequency of once per second as shown in Fig. 4(g). During 16 h of monitoring, the output power jitter is 0.59 mW, and the corresponding dispersion is 2.9%, indicating the durable and reliable effectiveness of the Bi_4Br_4 SA.

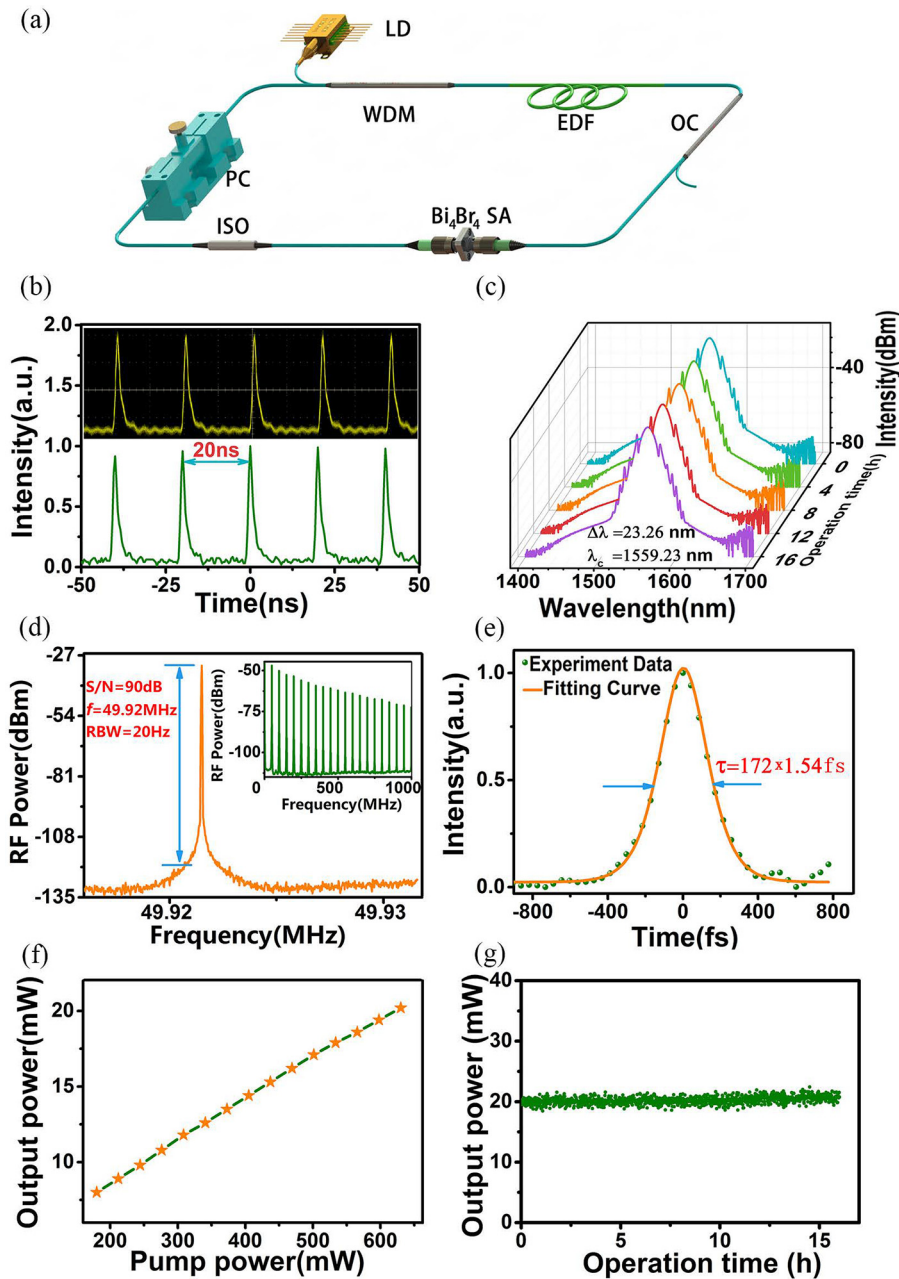


FIG. 4. Experimental setup and results of the MLFL. (a) The experimental schematic diagram of the ring cavity laser employing the Bi_4Br_4 -based SA. (b) Mode-locking phenomenon observed on the oscilloscope. (c) Optical spectrum. (d) The distribution of peaks in the radio frequency (RF) spectrum. (e) Pulse duration of solitons. (f) The output power plotted as a function of the pump power. (g) The jitter of the output power at a pump power of 630 mW.

After referring to the performance comparison in Table I, the laser employing the Bi_4Br_4 -based SA does not seem to be inferior to the laser based on other materials. The Bi_4Br_4 -based SA features the large modulation depth of 42.3%. The pulse duration of 172 fs obtained from the mode-locked laser highlights the potential of the Bi_4Br_4 -based SA in the realization of ultrafast pulses. From the values of the pump power and output power of various lasers in Table I, the conversion rate in power of the Bi_4Br_4 -based laser is decent. It is worth mentioning that it withstands higher pump power than other materials. Therefore, its durability at high power is worthy of recognition.

In conclusion, the optical nonlinearity of Bi_4Br_4 has been experimentally investigated here by a pulsed laser. The Bi_4Br_4 -based SA has featured the large modulation depth of 42.3% and played a key role in the realization of the mode-locked laser. The implemented mode-locked laser at 1559.23 nm has been characterized by a repetition frequency of 49.92 MHz, a SNR of 90 dB, and a pulse duration of 172 fs. Aside from that, the Bi_4Br_4 -based SA has indicated a strong resistance to the relatively high pump power and maintained robustness under long-term high-power excitation. The potential of Bi_4Br_4 in the development and innovation of nonlinear optics and ultrafast photonic

TABLE I. Comparison of ultrafast MLFLs based on some materials.

Materials	α_s^a	λ^b (nm)	τ^c (fs)	f_{rep}^d (MHz)	$P_{\text{pump}}/P_{\text{out}}$ (mW)	Efficiency	References
Graphene	65.9%	1561	1230	2.54	120/3	2.5%	24
Bi ₂ Se ₃	3.9%	1557.5	660	12.5	90/1.8	2%	35
Bi ₂ Te ₃	15.7%	1547	600	15.11	55/0.8	1.6%	36
BP	4.6%	1560.5	272	28.2	65/0.5	0.8%	37
MoS ₂	2.7%	1556.3	606	463	287/5.9	2%	38
WS ₂	2.9%	1572	595	25	310/4	1.3%	39
MoSe ₂	0.63%	1558.25	1450	8	50/0.4	0.8%	40
WTe ₂	2.85%	1556.2	770	13.98	25/0.04	0.2%	41
Bi ₄ Br ₄	42.3%	1559.23	172	49.92	630/20	3.2%	This work

devices operating in the near infrared and wider bands deserves to be focused and further explored.

This work was financially supported by the Beijing Natural Science Foundation (Nos. JQ21019 and Z190006), the National Natural Science Foundation of China (Nos. 11875008, 11974003, 11734003, and 12075034), the National Key Research and Development Program of China (No. 2020YFA0308800), the Open Research Fund of State Key Laboratory of Pulsed Power Laser Technology (Grant No. SKL2019KF04), and Fundamental Research Funds for the Central Universities (No. 2019XD-A09-3).

AUTHOR DECLARATIONS

Conflict of Interest

The authors have no conflicts to disclose.

DATA AVAILABILITY

The data that support the findings of this study are available from the corresponding authors upon reasonable request.

REFERENCES

- U. Keller, *Nature* **424**, 831 (2003).
- J. Su, L. Chai, W. Liu, and M. Hu, *IEEE J. Quantum Electron.* **55**, 1 (2019).
- A. H. Zewail, *Science* **242**, 1645 (1988).
- S. D. Jackson, *Nat. Photonics* **6**, 423 (2012).
- R. R. Gattass and E. E. Mazur, *Nat. Photonics* **2**, 219 (2008).
- C. Xu and F. W. Wise, *Nat. Photonics* **7**, 875 (2013).
- M. L. Liu, W. J. Liu, and Z. Y. Wei, *J. Lightwave Technol.* **37**, 3100 (2019).
- R. Y. Liao, Y. J. Song, and M. L. Hu, *Opt. Express* **27**, 14705 (2019).
- Y. W. Zhao, J. T. Fan, H. S. Shi, Y. P. Li, Y. J. Song, and M. L. Hu, *Opt. Express* **27**, 8808 (2019).
- W. Liu, R. Y. Liao, J. Zhao, J. H. Cui, Y. J. Song, C. Y. Wang, and M. L. Hu, *Optica* **6**, 194 (2019).
- Y. I. Jhon, J. Koo, B. Anasori, M. Seo, J. H. Lee, Y. Gogotsi, and Y. M. Jhon, *Adv. Mater.* **29**, 1702496 (2017).
- W. J. Liu, M. L. Liu, Y. Y. Ouyang, H. R. Hou, and Z. Y. Wei, *Nanotechnology* **29**, 394002 (2018).
- T. Jiang, K. Yin, C. Wang, J. You, H. Ouyang, and R. Miao, *Photonics Res.* **8**, 78 (2020).
- H. Zhang, D. Y. Zhao, L. M. Zhao, Q. L. Bao, and K. P. Loh, *Opt. Express* **17**, 17630 (2009).
- Z. Q. Luo, Y. Z. Huang, M. Zhong, Y. Y. Li, J. Y. Wu, B. Xu, H. Y. Xu, Z. P. Cai, J. Peng, and J. Weng, *J. Lightwave Technol.* **32**, 4679 (2014).
- M. Zhang, G. H. Hu, G. Q. Hu, R. C. T. Howe, L. Chen, Z. Zheng, and T. Hasan, *Sci. Rep.* **5**, 17482 (2015).
- R. L. Miao, Z. W. Shu, Y. Z. Hu, Y. X. Tang, H. Hao, J. You, X. Zheng, X. A. Cheng, H. G. Duan, and T. Jiang, *Opt. Lett.* **44**, 3198 (2019).
- C. X. Zhang, H. Ouyang, R. L. Miao, Y. Z. Sui, H. Hao, Y. X. Tang, J. You, X. Zheng, Z. J. Xu, X. A. Cheng, and T. Jiang, *Adv. Opt. Mater.* **7**, 1900631 (2019).
- W. J. Liu, L. H. Pang, H. N. Han, K. Bi, M. Lei, and Z. Y. Wei, *Nanoscale* **9**, 5806 (2017).
- W. J. Liu, M. L. Liu, H. N. Han, S. B. Fang, H. Teng, M. Lei, and Z. Y. Wei, *Photonics Res.* **6**, C15 (2018).
- M. Jung, J. Lee, J. Park, J. Koo, Y. M. Jhon, and J. H. Lee, *Opt. Express* **23**, 19996 (2015).
- J. Lee, Y. I. Jhon, K. Lee, Y. M. Jhon, and J. H. Lee, *Sci. Rep.* **10**, 15305 (2020).
- E. G. Mishchenko, *Phys. Rev. Lett.* **103**, 246802 (2009).
- Q. L. Bao, H. Zhang, Z. H. Ni, Y. Wang, L. Polavarapu, Z. X. Shen, Q. H. Xu, D. Y. Tang, and K. P. Loh, *Nano Res.* **4**, 297 (2011).
- M. Z. Hasan and C. L. Kane, *Rev. Mod. Phys.* **82**, 3045 (2010).
- P. G. Yan, R. Y. Lin, S. C. Ruan, A. J. Liu, and H. Chen, *Opt. Express* **23**, 154 (2015).
- H. J. Zhang, C. X. Liu, X. L. Qi, X. Dai, Z. Fang, and S. C. Zhang, *Nat. Phys.* **5**, 438 (2009).
- C. H. Hsu, X. T. Zhou, Q. Ma, N. Gedik, A. Bansil, V. M. Pereira, H. Lin, L. Fu, S. Y. Xu, and T. R. Chang, *2D Mater.* **6**, 031004 (2019).
- J. Zhou, W. Feng, G. B. Liu, and Y. Yao, *Nano Lett.* **14**, 4767 (2014).
- X. Li, D. Chen, M. Jin, D. Ma, and Y. Yao, *Proc. Natl. Acad. Sci.* **116**, 17696 (2019).
- J. Zhou, W. X. Feng, C. C. Liu, S. Guan, and Y. G. Yao, *New J. Phys.* **17**, 015004 (2015).
- W. J. Liu, M. L. Liu, X. Chen, T. Shen, M. Lei, J. G. Guo, H. X. Deng, W. Zhang, C. Q. Dai, X. F. Zhang, and Z. Y. Wei, *Commun. Phys.* **3**, 15 (2020).
- Y. Terada, S. Yoshida, O. Takeuchi, and H. Shigekawa, *J. Phys.-Condens. Mater.* **22**, 264008 (2010).
- Y. I. Jhon, J. Lee, Y. M. Jhon, and J. H. Lee, *IEEE J. Sel. Top. Quant.* **24**, 1102208 (2018).
- H. Liu, X. W. Zheng, M. Liu, N. Zhao, A. P. Luo, Z. C. Luo, W. C. Xu, H. Zhang, C. J. Zhao, and S. C. Wen, *Opt. Express* **22**, 6868 (2014).
- J. Lee, J. Koo, Y. M. Jhon, and J. H. Lee, *Opt. Express* **22**, 6165 (2014).
- J. Sotor, G. Sobon, W. Macherzynski, P. Paletko, and K. M. Abramski, *Appl. Phys. Lett.* **107**, 051108 (2015).
- K. Wu, X. Y. Zhang, J. Wang, and J. P. Chen, *Opt. Lett.* **40**, 1374 (2015).
- K. Wu, X. Y. Zhang, J. Wang, X. Li, and J. P. Chen, *Opt. Express* **23**, 11453 (2015).
- Z. Q. Luo, Y. Y. Li, M. Zhong, Y. Z. Huang, X. J. Wan, J. Peng, and J. Weng, *Photonics Res.* **3**, A79 (2015).
- J. Koo, Y. I. Jhon, J. Park, J. Lee, Y. M. Jhon, and J. H. Lee, *Adv. Funct. Mater.* **26**, 7454 (2016).